

# Solution Separation and Chi-Squared ARAIM for Fault Detection and Exclusion

Mathieu Joerges and Boris Pervan  
Illinois Institute of Technology  
Chicago, Illinois, U.S.A.

**Abstract**—Future multi-constellation Global navigation satellite system (GNSS) will provide a large number of redundant ranging signals, which will improve the performance of receiver autonomous integrity monitoring (RAIM), but it will also increase the probability of satellite faults, thereby increasing the continuity risk. In response, in this paper, a new Chi-Squared (Chi2) RAIM approach to fault detection and exclusion (FDE) is developed, and compared to Solution Separation (SS) RAIM. The paper first introduces complete integrity and continuity risk equations for Chi2 RAIM FDE, which are currently missing in the literature. Probability bounds are developed, which express the fact that the reduction in continuity risk obtained using exclusion comes at the cost of a higher integrity risk. It is then shown that the Chi2 approach can provide a tighter integrity risk bound as compared to SS, but the SS bound enables risk evaluation in practical implementations where computation resources are limited. Finally, the SS and Chi2 FDE integrity and continuity risk bounds are implemented to establish worldwide availability maps for Advanced RAIM (ARAIM) in an example aircraft approach application using GPS, Galileo, GLONASS and Beidou satellite constellations.

**Keywords**—GNSS; RAIM; ARAIM; fault detection and exclusion; multi-constellation

## I. INTRODUCTION

This paper describes the derivation, analysis and evaluation of a new fault detection and exclusion (FDE) method using chi-squared residual-based ( $\chi^2$ ) receiver autonomous integrity monitoring (RAIM). The paper builds upon prior work in [1], where a solution separation (SS) approach to RAIM FDE was developed. The SS and  $\chi^2$  approaches are the two most widely-implemented RAIM methods for fault detection. This paper provides complete integrity and continuity risk equations for  $\chi^2$  RAIM FDE, which extend the use of  $\chi^2$  RAIM to fault exclusion.

Global navigation satellite system (GNSS) measurements are vulnerable to rare-event faults including satellite failures, which can potentially lead to major integrity threats for users. To mitigate their impact, fault-detection algorithms such as RAIM can be implemented. RAIM exploits redundant ranging signals to achieve self-contained fault detection at the user receiver [2], [3]. With the modernization of GPS, the full deployment of GLONASS, and the emergence of Galileo and Beidou, the number of redundant ranging signals increases dramatically (as illustrated in Fig. 1), which opens the possibility to fulfill stringent navigation integrity requirements using RAIM. In particular, RAIM can help alleviate requirements on ground monitors. For example, researchers in

the European Union and in the United States are investigating Advanced RAIM (ARAIM) for worldwide vertical guidance of aircraft [4], [5].

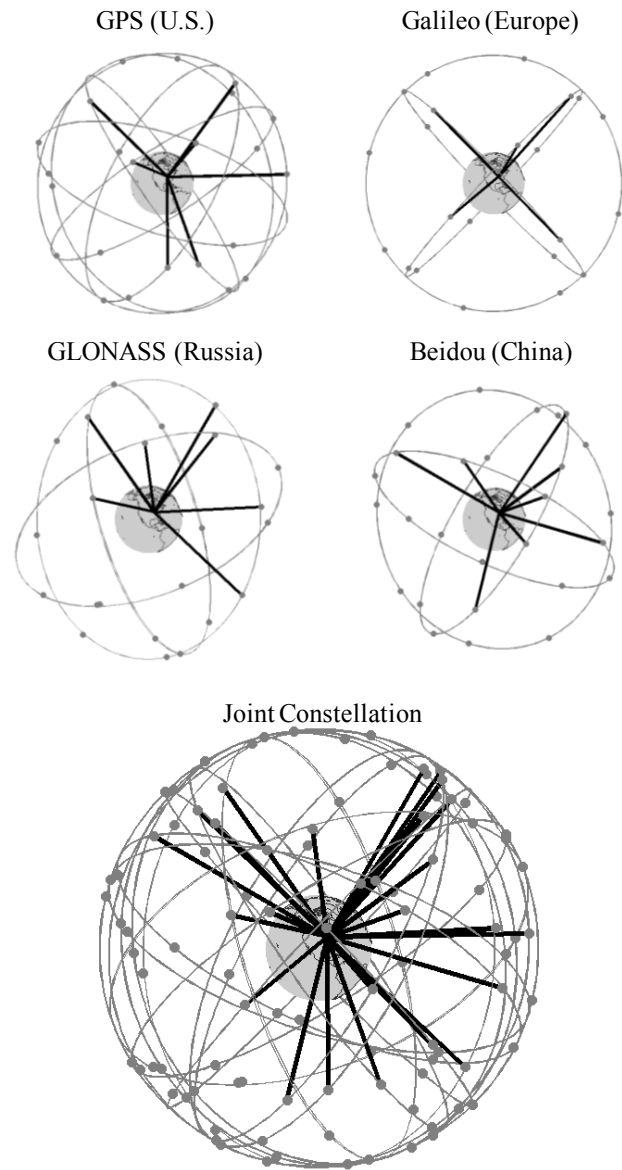


Fig. 1. Nominal satellite constellations for future GNSS

The authors gratefully acknowledge the Federal Aviation Administration (FAA) for supporting this research. However, the opinions expressed in this paper do not necessarily represent those of any other organization or person.

To further emphasize the impact of future multi-constellation GNSS on satellite redundancy, which is key to RAIM performance, Fig. 1 shows nominal satellite constellations for four GNSS. In this regard, it is worth reminding that using measurements from a single constellation, four satellites are needed for positioning, five are needed for RAIM-based fault detection, and six are needed for exclusion [6]. For each extra constellation included in the joint GNSS, an additional receiver clock bias must be determined, so that, for example, GPS/Galileo requires five SVs for positioning, six for detection and seven for exclusion. In Fig. 1, signals received at an example location (at Chicago, U.S.A.) are represented with thick black lines. Whereas each individual constellation only provides about five to ten ranging measurements, the joint constellation can provide continuous, global coverage of 25 to 35 satellites.

Two conflicting aspects of RAIM-based fault-detection arise from the addition of new redundant ranging signals in multi-constellation GNSS. On the one hand, the integrity monitoring performance using ARAIM is improving [4]. On the other hand, the heightened likelihood of satellite faults causes more occurrences of mission interruptions due to faults being detected, thereby increasing the continuity risk.

In response, fault exclusion procedures have been designed [4], [6], [7], which, unfortunately, do not provide the means to reliably predict the resulting integrity and continuity risks [8], [9]. Integrity risk evaluation is challenging because it involves quantifying the impact on state estimate errors of undetected faults and of wrong exclusions. A-priori integrity and continuity risk evaluation is needed when designing navigation systems to meet specific requirements, and it is needed operationally to predict if a mission (e.g., an aircraft approach) can be safely initiated. Without integrity and continuity risk equations for detection and exclusion, it remains unclear whether the overall navigation performance (including both integrity and continuity) will keep improving as the number of satellite signals increases.

Integrity risk evaluation is typically carried out using two different approaches in SS and  $\chi^2$  RAIM detection. In order to avoid making assumptions on the unknown fault distribution,  $\chi^2$  RAIM directly searches for the worst-case fault through the threat space [2], [3], whereas SS RAIM uses an integrity risk bounding process to formulate easy-to-compute protection levels (which are probabilistic bounds on the position estimate errors) [4], [8]. A detailed comparison of the two methods for detection only can be found in [15].

Integrity and continuity risk equations for SS RAIM FDE were established in [1]. The SS RAIM approach is briefly described in Sec. III, and motivates the derivation of a new  $\chi^2$  RAIM FDE method.

In Sec. IV, the  $\chi^2$  RAIM FDE method is developed based on parity space representations of a newly derived  $\chi^2$  RAIM exclusion test statistic. Parity space representations are instrumental because the parity vector, which can be used to derive both the SS and  $\chi^2$  test statistics [1], [10], is the simplest, most fundamental measure of fault detection capability. The paper will show that in parity space, the  $\chi^2$  RAIM no-detection and exclusion regions are hyper-spherical and cylindrical,

respectively, whereas for SS RAIM, they are polytopic and prismatic, respectively. Sec. IV also presents a complete derivation of the integrity and continuity risk equations for the  $\chi^2$  approach. These equations show that the reduction in continuity risk achieved using exclusion comes at the cost of a higher integrity risk. In parallel, a continuity risk bound is derived, which provides the means to determine detection and exclusion thresholds ensuring that the overall continuity risk requirement is satisfied.

Finally, in Sec. V, a performance analysis is carried out to assess worldwide availability of ARAIM FDE for an example aircraft approach navigation application using multi-constellation GNSS (assuming no constellation-wide faults and zero-mean nominal measurement errors). Availability maps are established, which confirm the analytical results of Sec. III and IV: on the one hand,  $\chi^2$  RAIM FDE provides tighter integrity and continuity risk bounds than SS RAIM FDE (because  $\chi^2$  RAIM directly searches through the threat space), but on the other hand, the SS bound enables risk evaluation in practical applications where computation resources are limited.

## II. BACKGROUND ON FAULT DETECTION USING RAIM

In this section, the integrity and continuity risks are first defined for fault detection only, followed by notations for the least-squares (LS) estimator. Then, the baseline detection test statistics for  $\chi^2$  RAIM and SS RAIM are derived, and represented in parity space for a canonical example. The content of this section is used in the remainder of the paper to analyze fault exclusion methods.

### A. Integrity and Continuity Risks for Fault Detection

The integrity risk criterion is defined in [11] as:

$$\sum_{i=0}^h P\left(|\varepsilon_0| > \ell, |q| < T \mid H_i\right) P_{H_i} \leq I_{REQ} - P_{NM} \quad (1)$$

where

- $\varepsilon_0$  is the error on the estimated parameter of interest (called ‘state’ of interest)
- $\ell$  is a specified alert limit that defines hazardous situations (e.g., specified in [12] for aircraft approach navigation)
- $q$  is the detection test statistic
- $T$  is the detection threshold
- $H_i$  for  $i = 0, \dots, h$  is a set of mutually exclusive, jointly exhaustive hypotheses.  $H_0$  is the fault-free hypothesis. The remaining  $h$  fault hypotheses correspond to faults on subset measurement ‘ $i$ ’ (including single-satellite and multi-satellite faults)
- $P_{H_i}$  is the prior probability of  $H_i$  occurrence
- $I_{REQ}$  is the integrity risk requirement (also specified in [12] for example aviation applications).

$P_{NM}$  is the prior probability of very rarely occurring faults that need not be monitored against (such that  $P_{NM} \ll I_{REQ}$ ). References [4] and [11] describe procedures to define the number  $h$  of fault hypotheses that must be monitored against, while conservatively accounting for the remaining fault combinations using their prior probability of occurrence  $P_{NM}$ .

The integrity risk, or probability of hazardous misleading information (HMI) noted  $P_{HMI}$ , refers here to the left hand side in (1).

Under the fault-free hypothesis  $H_0$ , the detection threshold  $T$  is typically set based on an allocated continuity risk requirement allocation  $C_{REQ0}$  (e.g., also specified in [12] for aviation applications) to limit the probability of false alarms [6]. For detection only,  $T$  can be defined as:

$$P(q \geq T | H_0) P_{H_0} \leq C_{REQ0} \quad (2)$$

In addition, let  $n$  and  $m$  respectively be the number of measurements and number of parameters to be estimated (i.e., the ‘states’). The  $n \times 1$  measurement vector  $\mathbf{z}_*$  is assumed normally distributed with covariance matrix  $\mathbf{V}_*$ . Vector  $\mathbf{z}_*$  is pre-multiplied by  $\mathbf{V}_*^{-1/2}$  to obtain the ‘normalized’ measurement equation:

$$\mathbf{z} = \mathbf{H}\mathbf{x} + \mathbf{v} + \mathbf{f} \quad (3)$$

where

- $\mathbf{z} = \mathbf{V}_*^{-1/2} \mathbf{z}_*$  is the normalized measurement vector
- $\mathbf{H}$  is the  $n \times m$  normalized observation matrix,
- $\mathbf{x}$  is the  $m \times 1$  state vector,
- $\mathbf{f}$  is the  $n \times 1$  normalized fault vector.
- $\mathbf{v}$  is the  $n \times 1$  normalized measurement noise vector composed of zero-mean, unit-variance independent and identically distributed (i.i.d.) random variables.

We use the notation:

$$\mathbf{v} \sim \mathbf{N}(\mathbf{0}_{n \times 1}, \mathbf{I}_n) \quad (4)$$

where

- $\mathbf{0}_{a \times b}$  is an  $a \times b$  matrix of zeros
- $\mathbf{I}_n$  is an  $n \times n$  identity matrix

In order to avoid making assumptions on unknown fault distributions, a bound on the probability of HMI given  $H_i$  can

be evaluated for the worst-case  $n \times 1$  fault vector  $\bar{\mathbf{f}}_i$ :

$$P\left(|\varepsilon_0| > \ell, |q| < T \mid H_i\right) \leq P\left(|\varepsilon_0| > \ell, |q| < T \mid \bar{\mathbf{f}}_i\right) \quad (5)$$

Vector  $\bar{\mathbf{f}}_i$  can be interpreted as a vector of deterministic measurement biases.

The worst-case fault vector  $\bar{\mathbf{f}}_i$ , which maximizes the integrity risk given  $H_i$ , is derived in [11] for multi-SV faults: the worst-case fault direction can be expressed analytically, and the worst-case magnitude is found using a straightforward line search algorithm. For the fault-free case ( $i = 0$ ), the following notation is used:  $\bar{\mathbf{f}}_0 = \mathbf{0}$ . The  $\chi^2$  RAIM approach directly uses the bound on the right hand side in (5), whereas in SS RAIM, a looser bound is typically implemented, which does not require determination of  $\bar{\mathbf{f}}_i$  (the SS bound is derived in Sec. III).

It has been proved in [10], [11] that  $\varepsilon_0$  and  $q$  are statistically independent ( $q$  is used here to represent both the  $\chi^2$  and the SS test statistics), so that the joint probability in (5) can be expressed as:

$$P\left(|\varepsilon_0| > \ell, |q| < T \mid \bar{\mathbf{f}}_i\right) = P\left(|\varepsilon_0| > \ell \mid \bar{\mathbf{f}}_i\right) P\left(|q| < T \mid \bar{\mathbf{f}}_i\right) \quad (6)$$

### B. Baseline Least-Squares Estimator Used in RAIM

This section defines the estimate error  $\varepsilon_0$  obtained using a least-squares (LS) estimator. Let  $x$  be the state of interest, for example the vertical position coordinate, which is often of primary concern for aircraft approach navigation. Let  $\alpha$  be an  $m \times 1$  vector used to extract  $x$  out of the full state vector:

$$\alpha^T = \begin{bmatrix} \mathbf{0}_{m_A \times 1}^T & 1 & \mathbf{0}_{m_B \times 1}^T \end{bmatrix}$$

where in the order in which states are stacked in  $\mathbf{x}$ ,  $m_A$  and  $m_B$  are the number of states respectively before and after state  $x$ . Assuming that  $\mathbf{H}$  is full rank and that  $n \geq m$ , the LS estimate of  $x$  is defined as:

$$\hat{x}_0 \equiv \mathbf{s}_0^T \mathbf{z} \quad (7)$$

$$\text{where } \mathbf{s}_0^T = \alpha^T \mathbf{P}_0 \mathbf{H}^T, \text{ and } \mathbf{P}_0 = (\mathbf{H}^T \mathbf{H})^{-1} \quad (8)$$

The LS estimate error appearing in (1) is defined as:

$$\varepsilon_0 \equiv \hat{x}_0 - x = \mathbf{s}_0^T (\mathbf{v} + \mathbf{f}) \quad (9)$$

$$\varepsilon_0 \sim \mathbf{N}(\mathbf{s}_0^T \mathbf{f}, \sigma_0^2 \equiv \alpha^T \mathbf{P}_0 \alpha) \quad (10)$$

### C. $\chi^2$ RAIM Detection Test Statistic

The  $\chi^2$  RAIM detection test statistic is derived from the  $(n-m) \times 1$  parity vector  $\mathbf{p}$ , which lies in the  $(n-m)$ -dimensional parity space, or left null space of  $\mathbf{H}$ , and can be expressed as [10], [13]:

$$\mathbf{p} \equiv \mathbf{Q}\mathbf{z} = \mathbf{Q}(\mathbf{v} + \mathbf{f}) \quad (11)$$

where the  $(n-m) \times n$  parity matrix  $\mathbf{Q}$  is defined as:

$$\mathbf{Q}\mathbf{Q}^T = \mathbf{I}_{n-m} \quad \text{and} \quad \mathbf{Q}\mathbf{H} = \mathbf{0}_{(n-m) \times m} \quad (12)$$

The  $\chi^2$  RAIM detection test statistic is the square of the norm of  $\mathbf{p}$ , and can be written as [10, 13]:

$$q_\chi^2 \equiv \mathbf{p}^T \mathbf{p} = \mathbf{r}^T \mathbf{r} \quad (13)$$

where  $\mathbf{r}$  is the LS residual vector defined as:

$$\mathbf{r} \equiv (\mathbf{I}_n - \mathbf{H}\mathbf{P}_0\mathbf{H}^T)\mathbf{z}. \quad (14)$$

$q_\chi^2$  follows a non-central chi-square distribution with  $(n-m)$  degrees of freedom and non-centrality parameter  $\lambda_\chi^2$  [10]. The following notation is used:

$$q_\chi^2 \sim \chi^2(n-m, \lambda_\chi^2) \quad (15)$$

where 
$$\lambda_\chi^2 = \mathbf{f}^T \mathbf{Q}^T \mathbf{Q} \mathbf{f} \quad (16)$$

### D. SS RAIM Detection Test Statistics

As an alternative to  $\chi^2$  RAIM, a second integrity monitoring method called SS RAIM [8], [14] is considered. Let  $n_i$  be the number of simultaneously faulted SVs under a given fault hypothesis  $H_i$ . Without loss of generality, it is assumed that under  $H_i$ , the faulty measurements are the first  $n_i$  elements of  $\mathbf{z}$ . The measurement equation (3) can be partitioned following the equation:

$$\begin{bmatrix} \mathbf{A}_i^T \mathbf{z} \\ \mathbf{B}_i^T \mathbf{z} \end{bmatrix} = \begin{bmatrix} \mathbf{A}_i^T \mathbf{H} \\ \mathbf{B}_i^T \mathbf{H} \end{bmatrix} \mathbf{x} + \begin{bmatrix} \mathbf{A}_i^T \mathbf{v} \\ \mathbf{B}_i^T \mathbf{v} \end{bmatrix} + \begin{bmatrix} \mathbf{A}_i^T \mathbf{f} \\ \mathbf{0}_{(n-n_i) \times 1} \end{bmatrix} \quad (17)$$

with 
$$\mathbf{A}_i \equiv \begin{bmatrix} \mathbf{I}_{n_i} \\ \mathbf{0}_{(n-n_i) \times n_i} \end{bmatrix} \quad \text{and} \quad \mathbf{B}_i \equiv \begin{bmatrix} \mathbf{0}_{n_i \times (n-n_i)} \\ \mathbf{I}_{n-n_i} \end{bmatrix} \quad (18)$$

Equation (17) is employed to distinguish the full-set solution  $\hat{\mathbf{x}}_0$  in (7), obtained using all  $n$  measurements in  $\mathbf{z}$ , from the subset solution  $\hat{\mathbf{x}}_i$ , derived using only the  $(n-n_i)$  *fault-free* measurements  $\mathbf{B}_i^T \mathbf{z}$  under  $H_i$ . Under the

assumption that  $n-n_i \geq m$ , and assuming that  $\mathbf{B}_i^T \mathbf{H}$  is full rank,  $\hat{\mathbf{x}}_i$  is defined as:

$$\hat{\mathbf{x}}_i \equiv \mathbf{s}_i^T \mathbf{z}, \quad \text{for } i=1, \dots, h \quad (19)$$

where  $\mathbf{s}_i^T \equiv \boldsymbol{\alpha}^T \mathbf{P}_i \mathbf{H}^T \mathbf{B}_i \mathbf{B}_i^T$ , and  $\mathbf{P}_i \equiv (\mathbf{H}^T \mathbf{B}_i \mathbf{B}_i^T \mathbf{H})^{-1}$  (20)

It follows that, under  $H_i$ , the estimate error  $\varepsilon_i$  is given by:

$$\varepsilon_i \equiv \mathbf{s}_i^T (\mathbf{v} + \mathbf{f}) \sim \mathcal{N}(0, \sigma_i^2 \equiv \boldsymbol{\alpha}^T \mathbf{P}_i \boldsymbol{\alpha}) \quad (21)$$

The solution separations are defined as [2], [8]:

$$\Delta_i \equiv \hat{\mathbf{x}}_0 - \hat{\mathbf{x}}_i = \varepsilon_0 - \varepsilon_i, \quad \text{for } i=1, \dots, h \quad (22)$$

$\Delta_i$  can also be expressed as [8], [14]:

$$\Delta_i = \mathbf{s}_{\Delta_i}^T \mathbf{z} \quad \text{and} \quad \Delta_i \sim \mathcal{N}(\mathbf{s}_{\Delta_i}^T \mathbf{f}, \sigma_{\Delta_i}^2) \quad (23)$$

where 
$$\mathbf{s}_{\Delta_i} \equiv \mathbf{s}_0 - \mathbf{s}_i \quad \text{and} \quad \sigma_{\Delta_i}^2 = \sigma_i^2 - \sigma_0^2 \quad (24)$$

Of particular significance in this work is the fact that for single-measurement faults, i.e., for  $n_i = 1$ ,  $\Delta_i$  can be written in terms of the parity vector  $\mathbf{p}$  as [1], [15]:

$$\Delta_i / \sigma_{\Delta_i} = \mathbf{u}_i^T \mathbf{p} \quad (25)$$

where 
$$\mathbf{u}_i \equiv \mathbf{Q} \mathbf{A}_i (\mathbf{A}_i^T \mathbf{Q}^T \mathbf{Q} \mathbf{A}_i)^{-1/2} \quad \text{for } i=1, \dots, h \quad (26)$$

with 
$$\mathbf{A}_i^T = \begin{bmatrix} \mathbf{0}_{(i-1) \times 1}^T & 1 & \mathbf{0}_{(n-i) \times 1}^T \end{bmatrix} \quad (27)$$

i.e.,  $\mathbf{Q} \mathbf{A}_i$  is the  $i^{\text{th}}$  column of  $\mathbf{Q}$ . Vector  $\mathbf{u}_i$  is the unit direction vector of the  $i^{\text{th}}$  ‘fault mode line’, which is the line described in parity space by the mean of  $\mathbf{p}$  as the magnitude of a fault on the  $i^{\text{th}}$  measurement varies from  $-\infty$  to  $+\infty$ . Parity space representations are introduced below. Equation (25) expresses the fact that the  $n$  solution separations (there are  $h = n$  solution separations when  $n_i = 1$ ) are projections of the parity vector on their corresponding fault mode lines.

### E. Parity Space Representations for a Canonical Example

In this section, both  $\chi^2$  RAIM and SS RAIM are represented in parity space for a canonical example used in [1], [10]. Let us consider a scalar state  $x$  and a  $3 \times 1$  measurement vector  $\mathbf{z}$  that are expressed as:

$$\mathbf{z} = \mathbf{H} x + \mathbf{v} + \mathbf{f} \quad (28)$$

where  $\mathbf{H} = [1 \ 1 \ 1]^T$  and  $\mathbf{v} \sim \mathcal{N}(\mathbf{0}_{3 \times 1}, \mathbf{I}_3)$  (29)

Since  $m=1$  and  $n=3$ , the  $(n-m)$  parity space is two-dimensional, which is convenient for display. The fault vector  $\mathbf{f}$  represents three single-measurement faults, corresponding to three fault hypotheses  $H_i$ , with unknown fault magnitude  $f_i$ .

$$\mathbf{f} = \begin{bmatrix} f_1 \\ 0 \\ 0 \end{bmatrix} \text{ or } \mathbf{f} = \begin{bmatrix} 0 \\ f_2 \\ 0 \end{bmatrix} \text{ or } \mathbf{f} = \begin{bmatrix} 0 \\ 0 \\ f_3 \end{bmatrix} \quad (30)$$

Their three fault mode lines, with direction vectors  $\mathbf{u}_i$  defined in (26), are represented in Fig. 2.

For  $\chi^2$  RAIM, the probability of no detection, which is the second term of the product in (6), is given by:  $P(q_\chi^2 < T_\chi^2 | \bar{\mathbf{f}}_i)$ . In contrast, for SS RAIM, the probability of no detection is a joint probability given by:

$$P(|\Delta_1| < T_1, |\Delta_2| < T_2, |\Delta_3| < T_3 | \bar{\mathbf{f}}_i) \quad (31)$$

It follows from (13), (25) and (31) that the detection boundaries for  $\chi^2$  and SS RAIM are a circle (or a hyper-sphere in higher-dimensional parity space) and a polygon (or a polytope), respectively. If the normalized SS detection thresholds are all equal ( $T_1 / \sigma_{\Delta 1} = T_2 / \sigma_{\Delta 2} = T_3 / \sigma_{\Delta 3}$ ), then the polygon is a hexagon.

If the measurement vector  $\mathbf{z}$  was noise-free and fault-free, the parity vector  $\mathbf{p}$  would be the null vector. However, because of the combined effect of  $\mathbf{v}$  and  $\mathbf{f}$ ,  $\mathbf{p}$  may land outside the detection boundary in Fig. 1., thereby establishing detection. Therefore, the probability of no detection is the probability of being inside the dash-dotted circle for  $\chi^2$  RAIM, and inside the hexagon for SS RAIM.

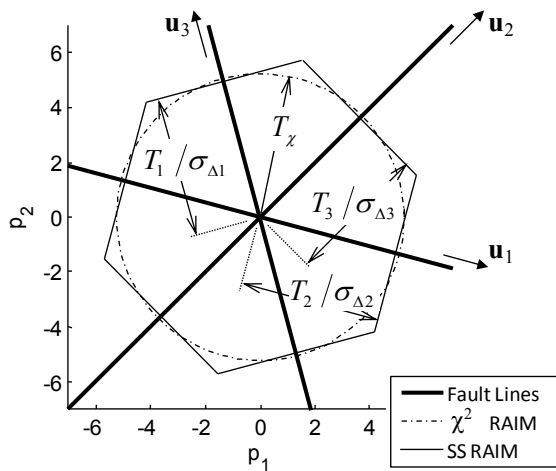


Fig. 2. Detection boundaries for  $\chi^2$  (circle) and SS (hexagon) in parity space

### III. SOLUTION SEPARATION RAIM FDE

This section describes the SS RAIM FDE method. Section III-A first defines general integrity and continuity risk equations for detection and exclusion (unlike Sec. II, which only addressed detection). These general definitions are later used in the development of both the SS and the  $\chi^2$  approach. In Sec. III-B, the SS RAIM FDE procedure is briefly outlined. Then, in Sec. III-C, new integrity and continuity risk equations for SS FDE are presented. Finally, Sec. III-D provides parity space representations, which set the basis for the derivation of the new  $\chi^2$  RAIM FDE method in Sec. IV.

#### A. General Integrity and Continuity Risk Equations

Sec. II was limited to fault detection algorithms. For detection only, the detection thresholds are typically set according to a continuity risk allocation  $C_{REQ0}$  to limit the probability of false alarms, as expressed in (2). However, the complete continuity risk accounts for all events causing a mission to be interrupted. These events not only include cases of detection under fault-free conditions (false alarms), but also cases of detection under faulted conditions. The complete continuity risk equation is given by:

$$P_{CONT} = P(D | H_0) P_{H_0} + \sum_{i=1}^h P(D | H_i) P_{H_i} \quad (32)$$

where  $D$  is the detection event.

If the detector is efficient, then the second term on the right hand side of (32) is approximately equal to the prior probability of any fault occurring:

$$\sum_{i=1}^h P(D | H_i) P_{H_i} \approx \sum_{i=1}^h P_{H_i} \quad (33)$$

If this probability is larger than the overall continuity risk requirement  $C_{REQ}$ , then faults need to be excluded to continue using the system.

This is why fault exclusion algorithms have been derived and implemented [4], [6], [7]. One crucial element that is missing in the literature, and that has been described as missing in [8] and [9], is a rigorous derivation of the integrity risk and continuity risk for RAIM FDE. In [1], we provided a preliminary integrity risk equation, which conservatively accounted for all fault and exclusion hypotheses.

In this paper, the definition of the integrity risk is refined to capture the fact that there can only be one exclusion hypothesis at a time. The word ‘exclusion’ is employed here to designate the choice of an estimator that uses a subset of measurements rather than the full set; other terms to replace the word exclusion have been employed in the literature, including ‘isolation’ and ‘reconfiguration’ [6]. The integrity risk bound for fault detection and exclusion is defined as:

$$P_{HMI} \leq \sum_{i=0}^h P(HI_0, ND | H_i) P_{Hi} + \sum_{j=1}^h \sum_{i=0}^h P(HI_j, D, E_j | H_i) P_{Hi} \quad (34)$$

where

- $HI_j$  : hazardous information using the LS estimator  $\mathbf{s}_j$ , defined in (8) for the full-set solution  $\mathbf{s}_0$ , and in (20) for subset solutions  $\mathbf{s}_j$ ,  $j \neq 0$
- $ND$  : no detection
- $E_j$  : exclusion of measurement subset  $j$

The first term in (34) is the same as the integrity risk for detection only given in (2). The second term accounts for the risk of performing an exclusion: it is the price to pay in terms of integrity risk for reducing the continuity risk using exclusion. It accounts for all fault hypotheses (subscript  $i$ ), and all exclusion candidates (subscript  $j$ ).

In parallel, the continuity risk is redefined to express that mission interruptions occur if a fault is detected, but cannot be excluded:

$$P_{CONT} \equiv \sum_{i=0}^h P(D, NE | H_i) P_{Hi} \quad (35)$$

where  $NE$  is the ‘no exclusion’ event.

### B. Solution Separation FDE Exclusion Procedure

To understand how no-exclusion events can occur, we present an example three-step SS exclusion procedure:

- The first step is the SS detection tests described in Sec. II. A fault is detected if:

$$|\Delta_k| \equiv |\varepsilon_0 - \varepsilon_k| \geq T_k \quad \text{for any } k, k=1, \dots, h \quad (36)$$

- In case of detection, multiple exclusion candidates are considered, i.e., estimators are evaluated, which use all measurements except candidate subset ‘ $j$ ’, for  $j=1, \dots, h$ . The resulting subset solution using all remaining measurements after exclusion is noted  $\varepsilon_j$ . In order to find  $\varepsilon_j$  that can be assumed fault free, we carry out a second layer of detection using all subset solutions  $\varepsilon_{j,l}$  within the selected candidate subset solution  $\varepsilon_j$ . Thus, a subset ‘ $j$ ’ is excluded only if

$$|\Delta_{j,l}| \equiv |\varepsilon_j - \varepsilon_{j,l}| < T_{j,l} \quad \forall l, \begin{cases} l=1, \dots, h \\ \forall \text{ subsets } l \subset \text{subset } j \end{cases} \quad (37)$$

where  $\varepsilon_{j,l}$  is the subset solution that excludes both measurement subsets  $j$  and  $l$ .

- Finally, if the exclusion test in (37) passes, then  $\varepsilon_j$  can be used for positioning and (34) can be used to bound the actual integrity risk. Conversely, if any one of the exclusion tests in (37) triggers for each of the candidate subset solutions  $\varepsilon_j$ , for  $j=1, \dots, h$ , then the mission is interrupted. This case is accounted for in the continuity risk equation in (35).

Let  $\tau_j$  be the number of exclusion tests needed to validate  $\varepsilon_j$  in (37).  $\tau_j$  is given by

$$\tau_j = h - \sum_{k=1}^{n_j} C_k^{n_j} \quad (38)$$

where  $C_k^n$  is the binomial coefficient. For single-SV faults (i.e., when  $n_j=1$ , for  $j=1, \dots, h$ ), we get a much simpler expression:  $\tau_j = h-1 = n-1$ , under  $H_j$ . To simplify the upcoming comparison of SS RAIM versus  $\chi^2$  RAIM with respect to the number  $\tau_j$  of exclusion test statistics, the discussion is carried out for single-SV faults. In this case, the total number of SS detection and exclusion tests is  $h^2$ . Multi-SV faults can still be fully accounted using the integrity and continuity risk equations derived below.

### C. Integrity and Continuity Risk Bounds for Solution Separation FDE

Integrity risk evaluation using (34) is challenging because the estimation error and the detection and exclusion test statistics in the joint probabilities are correlated. In response, an upper bound on  $P_{HMI}$  is derived in [1]. The derivation is valid for estimators other than the least squares estimator and is not restricted to single measurement faults. The resulting integrity risk bound is expressed as:

$$P_{HMI} \leq P(\varepsilon_0 > \ell | H_0) P_{H0} + \sum_{i=1}^h P(\varepsilon_i + T_i > \ell | H_i) P_{Hi} + \sum_{j=1}^h \left( \sum_{S_i \subset S_j} P(\varepsilon_j > \ell | H_i) P_{Hi} + \sum_{S_i \not\subset S_j} P(\varepsilon_{j,i} + T_{j,i} > \ell | H_i) P_{Hi} \right) \quad (39)$$

This bound on  $P_{HMI}$  is independent of the fault vector (which will not be the case in  $\chi^2$  RAIM). The first two terms on

the right hand side of (39) are a bound on the probability of hazardous information and no detection. An equivalent protection level formulation for these terms is typically used for  $P_{HMI}$  evaluation in SS RAIM using detection only [4], [8], [14]. The third term on the right hand side of (39) accounts for all cases of hazardous information, detection, and exclusion. The first term within this sum is a bound on the probability of excluding a subset  $S_j$  that includes the faulted subset  $S_i$  ( $S_i \subset S_j$ ). This term incorporates the fault-free hypothesis  $H_0$ , for which the notation  $S_0$  designates an empty subset included in all  $S_j$ , for  $j=1, \dots, h$ . The second term under the  $j$ -indexed sum is a bound on the probability of wrong exclusion (defined as  $S_i \not\subset S_j$ ) under faulty conditions.

The integrity risk bound in (39) is designed to enable risk evaluation in implementations where computational resources are limited. Key conservative assumptions required to obtain (39) are highlighted in [1]. These assumptions will later explain why  $\chi^2$  RAIM is expected to provide a tighter integrity risk bound than SS RAIM.

In addition, in [1], a bound on the continuity risk  $P_{CONT}$  is derived, which is expressed as:

$$P_{CONT} \leq \sum_{i=1}^h P(|\Delta_i| \geq T_i | H_0) P_{H_0} + \sum_{j=1}^h \sum_{\substack{i=1 \\ S_i \not\subset S_j}}^h P(|\Delta_{j,i}| \geq T_{j,i} | H_0) P_{H_i} \quad (40)$$

This equation is crucial because it provides the means to determine the  $h$  detection thresholds and the  $h(h-1)$  exclusion thresholds, while ensuring that the overall continuity risk requirement  $C_{REQ}$  is met.

The detection and exclusion thresholds can be written as:

$$T_i = Q^{-1} \left\{ \beta \frac{C_{REQi}}{2P_{H_0}} \right\} \sigma_{\Delta_i} \quad (41)$$

$$T_{j,i} = Q^{-1} \left\{ \alpha_{j,i} (1-\beta) \frac{C_{REQi}}{2P_{H_i}} \right\} \sigma_{\Delta_{j,i}} \quad (42)$$

where

$Q^{-1}\{\}$  is the inverse tail probability distribution of the two-tailed standard normal distribution ( $Q\{\} = 1 - \Phi\{\}$ , where  $\Phi\{\}$  is the standard normal cumulative distribution function).

$\sigma_{\Delta_{j,i}}^2 = \sigma_{j,i}^2 - \sigma_j^2$ , and  $\sigma_{j,i}$  is the standard deviation of the subset solution that excludes both the  $i$  and  $j$  measurement subsets

and where the continuity risk allocation can be performed considering the following equations:

$$C_{REQ} = \sum_{i=1}^h C_{REQi}, \quad \text{e.g., } C_{REQi} = C_{REQ}/h \quad (43)$$

$$0 < \beta \leq 1, \quad \text{e.g., } \beta = 1/2 \quad (44)$$

$$\sum_{j=1}^{h-1} \alpha_{j,i} = 1 \quad \text{e.g., } \alpha_{j,i} = 1/(h-1) \quad (45)$$

#### D. Parity Space Representation of SS RAIM FDE

The no-detection and exclusion regions were represented in [1] by sampling the parity space and identifying points passing the detection and exclusion tests in (36) and (37). These results are repeated here to facilitate the comparison with  $\chi^2$  RAIM in Sec. IV of this paper.

For the canonical example given in Sec. II-E, the no-detection and exclusion regions are displayed in Fig. 3. First, we can recognize the fair-gray, hexagonal SS-based no-detection area introduced earlier in Fig. 2. Then, Fig. 3 shows that the SS exclusion areas (dark gray) are bands surrounding the fault mode lines. These bands are sensible criteria for exclusion. If the parity vector is near a fault line, then it is easy to figure out which measurement to exclude. On the contrary, if the parity vector lands in between two fault mode lines, then it becomes extremely challenging to determine which of the two fault modes caused the error that was detected, and it is safer not to exclude.

Exclusion regions can also be represented in higher-dimensional parity space. For example, to obtain a three-dimensional parity space representation, the measurement vector  $\mathbf{z}$  in (28) is augmented with one additional measurement, so that the observation matrix becomes:

$$\mathbf{H} = [1 \ 1 \ 1 \ 1]^T \quad (46)$$

The  $4 \times 1$  measurement noise vector  $\mathbf{v}$  is still zero-mean normally distributed with covariance  $\mathbf{I}_4$  and the  $4 \times 1$  fault vector now includes one additional single-measurement fault mode.

The resulting no-detection and exclusion spaces are respectively shown in fair gray and dark gray in Fig. 4. Focusing on a single fault mode and looking at a plane normal to the corresponding fault mode line reveals the shape of the SS exclusion region, which is displayed in Fig. 5. For each fault hypothesis, SS RAIM uses  $(h-1)$  test statistics to define an exclusion region. The advantage of these SS test statistics is that they are normally distributed, which is convenient for practical risk evaluation using the protection levels derived in [1].

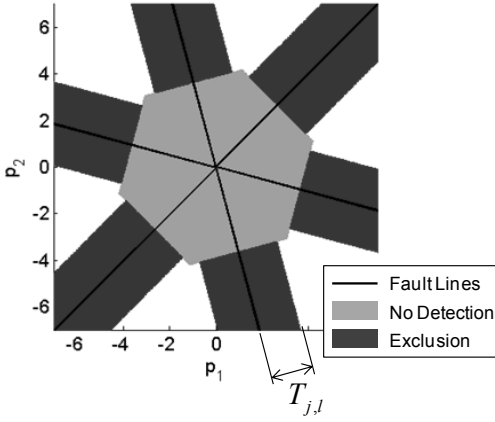


Fig. 3. No-detection and exclusion areas for SS RAIM in two dimensional parity space

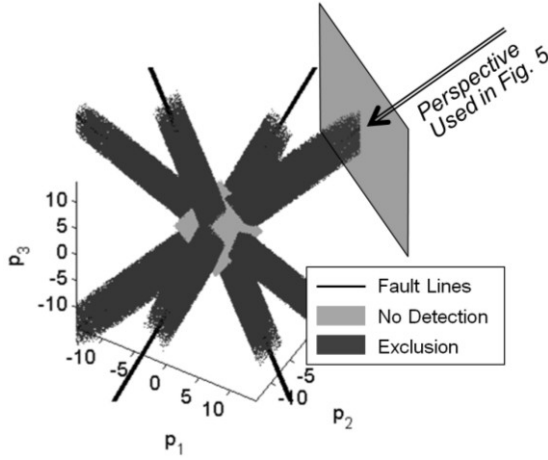


Fig. 4. No-detection and exclusion zones for SS RAIM in three dimensional parity space

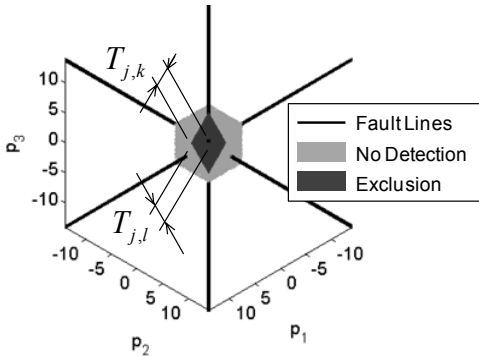


Fig. 5. Visualization of the SS RAIM exclusion region

However, it can seem inefficient to use  $(h-1)$  SS exclusion tests for each of the  $h$  exclusion candidates to generate the regions surrounding the fault lines. Instead, a single test per fault hypothesis should be enough to define, for example, a cylindrical exclusion region around the fault line. This idea motivated the derivation of a  $\chi^2$  RAIM FDE method in Sec. IV.

#### IV. CHI-SQUARED RESIDUAL-BASED FDE

In this section, a new  $\chi^2$  RAIM FDE method is developed. First, Sec. IV-A presents the derivation of the new  $\chi^2$  RAIM exclusion test statistics, which are measures of the distance between the parity vector and the fault lines. The derivation deals with cases of multiple simultaneous SV faults. Then, Sec. IV-B and IV-C establish the  $\chi^2$  RAIM FDE integrity and continuity risk equations. Finally, parity space representations for this new method are provided.

##### A. Definition of the $\chi^2$ RAIM Exclusion Test Statistic

Following the observations made at the end of Sec. III, a  $\chi^2$  RAIM exclusion test statistic is derived, which provides a measure of the distance to the fault line. To achieve this, we determine the projection of the parity vector  $\mathbf{p}$  (defined in (11)) on the plane normal to the fault line with unit direction vector  $\mathbf{u}_j$  (defined in (26)) under fault hypothesis  $H_j$ . The projected vector is expressed as:

$$\mathbf{q}_{\perp,j} \equiv [\mathbf{I}_{n-m} - \mathbf{U}_j \mathbf{U}_j^T] \mathbf{p} = \mathbf{M}_{\perp,j} \mathbf{z} \quad (47)$$

where 
$$\mathbf{U}_j \equiv \mathbf{Q} \mathbf{A}_j (\mathbf{A}_j^T \mathbf{Q}^T \mathbf{Q} \mathbf{A}_j)^{-1/2} \quad (48)$$

$$\mathbf{M}_{\perp,j} \equiv [\mathbf{I}_{n-m} - \mathbf{U}_j \mathbf{U}_j^T] \mathbf{Q} \quad (49)$$

The  $(n-m) \times (n-m)$  matrix  $[\mathbf{I}_{n-m} - \mathbf{U}_j \mathbf{U}_j^T]$  is an orthogonal projection operator [16]. The  $(n-m) \times n_j$  matrix  $\mathbf{U}_j$  (instead of  $\mathbf{u}_j$  for single-SV faults) provides the means to define  $\mathbf{q}_{\perp,j}$  under mutli-SV fault hypotheses. (As a reminder,  $n_j$  is defined in (17) as the number of simultaneously faulted SVs under  $H_j$ .)

The  $\chi^2$  RAIM exclusion test statistic is defined as:

$$q_{\perp,j}^2 \equiv \mathbf{q}_{\perp,j}^T \mathbf{q}_{\perp,j} \quad (50)$$

$$q_{\perp,j}^2 \sim \chi^2(\mathbf{f}^T \mathbf{M}_{\perp,j}^T \mathbf{M}_{\perp,j} \mathbf{f}, n-m-n_j) \quad (51)$$

Similar to the detection statistic  $q_{\chi}^2$  in (13), the exclusion statistic can be directly expressed in terms of the residual vector  $\mathbf{r}$ , and of matrices  $\mathbf{H}$  and  $\mathbf{P}_0$ :

$$q_{\perp,j}^2 = \mathbf{r}^T \left( \mathbf{I}_n - \mathbf{A}_j \left( \mathbf{A}_j^T (\mathbf{I} - \mathbf{H}\mathbf{P}_0 \mathbf{H}^T) \mathbf{A}_j \right)^{-1} \mathbf{A}_j^T \right) \mathbf{r} \quad (52)$$

Proof of this result is given in Appendix I.

The  $\chi^2$  RAIM FDE procedure is identical to the SS approach described in Sec. III-B, with the detection and exclusion test statistics  $q_\chi^2$  and  $q_{\perp,i}^2$  respectively replacing  $|\Delta_k|$  and  $|\Delta_{j,i}|$ . Also, for single-SV faults, the total number of detection and exclusion tests drops from  $h^2$  for SS RAIM to  $h+1$  for  $\chi^2$  RAIM.

### B. Integrity Risk Bound for $\chi^2$ RAIM FDE

A bound on the  $\chi^2$  RAIM FDE integrity risk is derived from the general  $P_{HMI}$  equation in (34). First, the following inequality is considered (also used for SS RAIM in [1]):

$$P(HI_j, D, E_j | H_i) \leq P(HI_j, E_j | H_i) \quad (53)$$

Then, a worst-case approach, similar to the one used in (5) for detection only, is implemented to evaluate the impact of faults. The definitions of the events  $HI_0$ ,  $ND$ ,  $HI_j$ , and  $E_j$  for  $\chi^2$  RAIM are directly used to establish an integrity risk bound that can be written as:

$$P_{HMI} \leq \sum_{i=0}^h P(\varepsilon_0 > \ell | \bar{\mathbf{f}}_i) P(q_\chi^2 < T_\chi^2 | \bar{\mathbf{f}}_i) P_{Hi} \\ + \sum_{j=1}^h \sum_{i=0}^h P(\varepsilon_j > \ell | \bar{\mathbf{f}}_{\perp,j,i}) P(q_{\perp,j}^2 < T_{\perp,j}^2 | \bar{\mathbf{f}}_{\perp,j,i}) P_{Hi} \quad (54)$$

The worst case fault direction for exclusion is derived in Appendix II and can be expressed as:

$$\bar{\mathbf{f}}_{\perp,j,i} = \mathbf{A}_i \left( \mathbf{A}_i^T \mathbf{M}_{\perp,j}^T \mathbf{M}_{\perp,j} \mathbf{A}_i \right)^{-1} \mathbf{A}_i^T \mathbf{s}_j \quad (55)$$

$$\text{or,} \quad \bar{\mathbf{f}}_{\perp,j,i} = \mathbf{A}_i \left( \mathbf{A}_i^T \mathbf{R}_j \mathbf{A}_i \right)^{-1} \mathbf{A}_i^T \mathbf{s}_j \quad (56)$$

where

$$\mathbf{R}_j \equiv (\mathbf{I} - \mathbf{H}\mathbf{S}_0) \left( \mathbf{I} - \mathbf{A}_j \left( \mathbf{A}_j^T (\mathbf{I} - \mathbf{H}\mathbf{S}_0) \mathbf{A}_j \right)^{-1} \mathbf{A}_j^T \right) (\mathbf{I} - \mathbf{H}\mathbf{S}_0) \quad (57)$$

In addition, (54) exploits the fact, proved in Appendix III, that  $\varepsilon_j$  and  $q_{\perp,j}^2$  are statistically independent. Statistical independence between estimate error and test statistic, which is only achievable using LS estimators [11], is required here to evaluate the terms in (54) as products of probabilities. This constraint on the estimator for  $\chi^2$  RAIM is not imposed on SS RAIM, which instead evaluates  $P_{HMI}$  using a bounding process outlined in [1].

Finally, the  $\chi^2$  RAIM integrity risk bound in (54) does not require the conservative assumptions made in [1], so that  $\chi^2$

RAIM provides a tighter  $P_{HMI}$  bound than SS RAIM. Also, (54) only uses  $h+1$  test statistics, versus  $h^2$  for SS RAIM. However, in  $\chi^2$  RAIM, although the worst-case fault direction is given by (55), the worst-case fault magnitude still needs to be determined using a line-search algorithm. This search process ultimately causes  $\chi^2$  RAIM to be computationally more expensive than SS RAIM.

### C. Continuity Risk Bound for $\chi^2$ Residual-Based FDE

The  $\chi^2$  RAIM FDE continuity risk bound is derived in two steps, based on the general continuity risk definition in (35). First, the term of the sum corresponding to the fault-free hypothesis in (35) is rewritten as:

$$P(D, NE | H_0) = P(q_\chi^2 \geq T_\chi^2, q_{\perp,1}^2 \geq T_{\perp,1}^2, \dots, q_{\perp,h}^2 \geq T_{\perp,h}^2 | H_0) \\ \leq P(q_\chi^2 \geq T_\chi^2 | H_0) \quad (58)$$

Then, the remaining terms are addressed using the following inequality:

$$P(D, NE | H_i) = P(q_\chi^2 \geq T_\chi^2, q_{\perp,1}^2 \geq T_{\perp,1}^2, \dots, q_{\perp,h}^2 \geq T_{\perp,h}^2 | H_i) \\ \leq P(q_{\perp,i}^2 \geq T_{\perp,i}^2 | H_i) \quad (59)$$

Substituting (58) and (59) into (35), the  $\chi^2$  RAIM continuity risk bound can be expressed as:

$$P_{CONT} \leq P(q_\chi^2 \geq T_\chi^2 | H_0) P_{H0} + \sum_{i=1}^h P(q_{\perp,i}^2 \geq T_{\perp,i}^2 | H_0) P_{Hi} \quad (60)$$

The detection thresholds can therefore be written as:

$$T_\chi^2 = \chi^{-2} \left\{ 1 - \beta \frac{C_{REQ}}{P_{H0}}, n - m \right\} \quad (61)$$

$$T_{\perp,j}^2 = \chi^{-2} \left\{ 1 - (1 - \beta) \frac{C_{REQ}}{P_{Hj}}, n - m - n_j \right\} \quad (62)$$

where  $\beta$  was defined in (44) and  $\chi^{-2}\{P, \delta\}$  is the inverse cumulative distribution function of the chi-square distribution with  $\delta$  degrees of freedom at the probability value  $P$ .

The continuity risk requirement is allocated between  $(h+1)$  test statistics for  $\chi^2$  RAIM, versus  $h^2$  statistics for SS RAIM, which would suggest that the continuity risk requirement can be more efficiently satisfied using  $\chi^2$  RAIM. However, the comparison in terms of continuity risk is more subtle because the  $\chi^2$  RAIM test statistics are chi-squared distributed whereas the SS test statistics are normally distributed. Further discussion on this topic, for detection only, is given in [1], [15], [17].

#### D. Parity Space Representation of $\chi^2$ RAIM FDE

Parity space representations are directly obtained by sampling the parity space and identifying the points that satisfy the detection and exclusion tests. For the three dimensional canonical example described in Sec. III-D, Fig. 6 and 7 display the fair-gray spherical no-detection region at the origin, and the dark-gray cylindrical exclusion regions surrounding the faults lines. These regions are analogous to the SS RAIM polytopic and prismatic detection and exclusion regions shown in Fig. 4 and 5. Fig. 6 and 7 confirm that the  $\chi^2$  RAIM exclusion test statistic  $q_{\perp,i}^2$  defined in (50) accomplishes the objective set at the beginning of this section of obtaining a cylindrical exclusion region using a single test statistic.

#### V. PERFORMANCE EVALUATION

Sec. IV has shown that  $\chi^2$  RAIM enables direct integrity risk evaluation (in (54)) using  $(h+1)$  detection and exclusion test statistics defined in (13) and (50), but requires that the worst-case fault magnitudes for  $\bar{\mathbf{f}}_i$  and  $\bar{\mathbf{f}}_{\perp,j,i}$  be determined. In contrast, SS RAIM uses  $h^2$  test statistics defined in (22) and (37) to provide a looser integrity risk bound given in (39), which is independent of fault magnitudes, thereby enabling computationally efficient implementations.

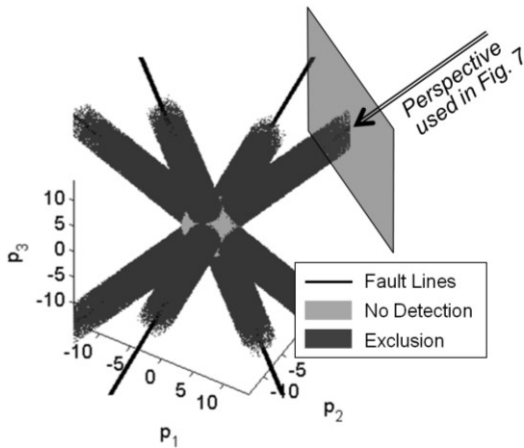


Fig. 6. No-detection and exclusion zones for  $\chi^2$  RAIM in three dimensional parity space

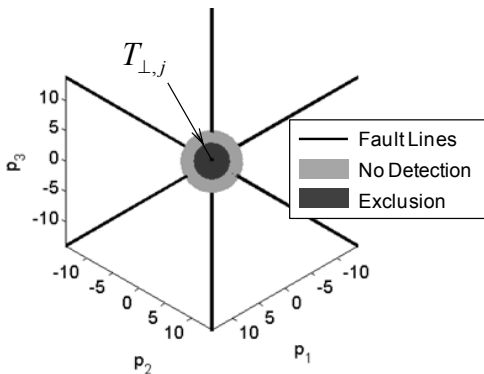


Fig. 7. Visualization of the  $\chi^2$  RAIM exclusion region

TABLE I. SIMULATION PARAMETERS

Parameter	Value			
	GPS	Galileo	GLO NASS	Beidou
SV clock, orbit error (URA)	0.75 m	0.96 m	1m	1m
Residual tropo. error <sup>a</sup>	$0.12 \frac{1.001}{(0.002001 + \sin^2 \xi)^{1/2}}$ m			
Smoothed code multipath <sup>a</sup>	$0.13 + 0.53e^{-\xi/10}$ m	lookup table [4]	same as GPS	same as GPS
Smoothed code receiver noise <sup>a</sup>	$0.15 + 0.43e^{-\xi/6.9}$ m			
Fault-free range bias $b_{MAX}$	0 m			
$I_{REQ}$	$10^{-7}$			
$C_{REQ}$	$2 \cdot 10^{-6}$			
$P_{Hi}$	$10^{-5}$	$10^{-5}$	$10^{-5}$	$10^{-5}$
Constellation-wide faults	none considered			

<sup>a</sup>.  $\xi$  is the satellite elevation angle in degrees

This section aims at quantifying the reduction in integrity risk obtained using  $\chi^2$  RAIM versus SS RAIM, and at assessing the difference in processing time between the two methods.

#### A. Benchmark ARAIM Application, Requirements and Measurement Error Models

The SS and  $\chi^2$  RAIM FDE methods derived in the previous sections are evaluated in an example Advanced RAIM (ARAIM) application for vertical guidance of aircraft using dual-frequency GPS, Galileo, GLONASS and Beidou. The simulation parameters, which include ARAIM measurement error models, and LPV-200 navigation requirements (to support localizer precision vertical aircraft approach operations down to 200 feet above the ground), are listed in Table I and described in detail in [4], [5]. In this preliminary performance evaluation, in order to be consistent with (4), we assume zero mean nominal measurement errors. The complete ARAIM error model, which assumes non-zero mean errors bounded by a nominal bias labeled  $b_{MAX}$ , will be further analyzed in future work.

Sensitivity to the alert limit  $\ell$  is evaluated for values ranging from 10 m to from 35 m. The nominal satellite constellations used in this work include 24 GPS satellites [18], 24 Galileo satellites [19], 23 GLONASS satellites and 27 Beidou satellites [20]. Moreover, this analysis focuses on the vertical position coordinate, for which the aircraft approach navigation requirements are often the most difficult to fulfill (the LPV 200 vertical alter limit requirement  $\ell$  is 35).

#### B. Integrity Risk Evaluation

In Fig. 8, the integrity risk  $P_{HMI}$  is evaluated over 24 hours at an example Chicago location, for an example vertical alert limit  $\ell$  of 10 m, for the joint GPS / Galileo system. The bounds for  $\chi^2$  and SS RAIM are respectively displayed with a thick, solid line and with a dotted line with black diamond

markers. Despite a tight 10 m alert limit  $\ell$ , the two curves are mostly below the  $10^{-7}$  integrity risk requirement  $I_{REQ}$ , which is optimistic because, in this preliminary analysis, the fault-free measurement bias  $b_{MAX}$  is assumed to be zero. The focus in Fig. 8 is on the comparison between  $\chi^2$  and SS RAIM. In this regard, the  $\chi^2$  RAIM curve is significantly lower than the SS RAIM curve, achieving  $P_{HMI}$  values five to ten times lower than for SS RAIM. The fact that the  $\chi^2$  approach provides a tighter integrity risk bound than SS RAIM confirms the theoretical analysis of Sec. III and IV.

### C. Preliminary Worldwide Availability Evaluation and Sensitivity Analysis

To further quantify the difference between  $\chi^2$  and SS RAIM FDE, availability maps are presented in Fig. 9 and 10 for an example 15 m alert limit  $\ell$ , for a 10 deg  $\times$  10 deg latitude-longitude grid of locations, for GPS/Galileo satellite geometries simulated at regular ten minute intervals over a 24 hour period. Availability is computed at each location as the fraction of time where the  $P_{HMI}$  bound meets the integrity risk requirement  $I_{REQ}$ . In Fig. 9 and 10, availability is color-coded: white color corresponds to a value of 100%, black represents 98%. Constant availability contours are also displayed for 99% and 100% probability levels. Fig. 9 clearly shows darker areas corresponding to lower availability for SS RAIM FDE as compared to  $\chi^2$  RAIM FDE in Fig. 10.

The worldwide availability metric given in the figure captions is the weighted coverage of 99.9% availability: the coverage is defined as the percentage of grid point locations exceeding 99.9% availability; the coverage computation is weighted at each location by the cosine of the location's latitude, because grid point locations near the equator represent larger areas than near the poles. Fig. 9 and 10 show that the coverage of 99.9% availability increases from 85.04% for SS RAIM, to 93.44% for  $\chi^2$  RAIM, assuming  $\ell = 15$  m.

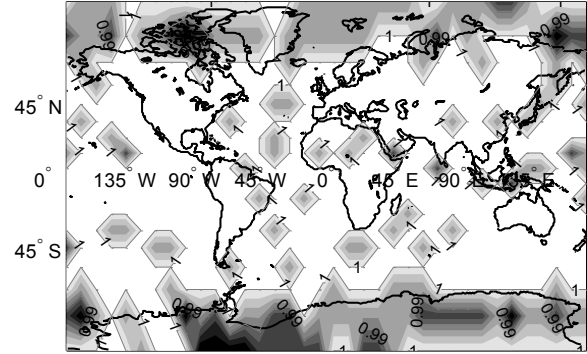


Fig. 9. Availability map for SS RAIM using GPS/Galileo, for  $b_{MAX}=0$ , for an alert limit of 15 m (coverage of 99.9% availability is 85.04%).

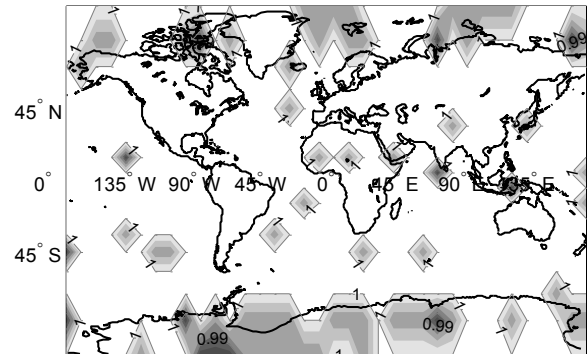


Fig. 10. Availability map for  $\chi^2$  RAIM using GPS/Galileo, for  $b_{MAX}=0$ , for an alert limit of 15 m (coverage of 99.9% availability is 93.44%).

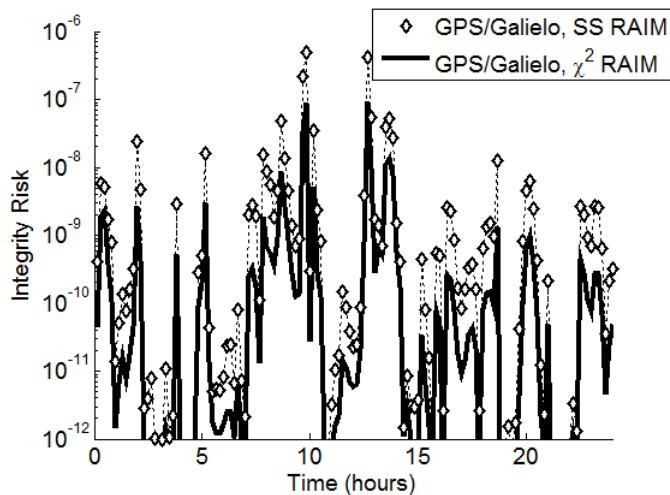


Fig. 8. Integrity risk evaluated using SS and  $\chi^2$  RAIM over 24 hours at the Chicago location, for  $b_{MAX}=0$ , for an example alert limit of 10 m.

The sensitivity of worldwide coverage to  $\ell$  is further evaluated in Fig. 11, for values of  $\ell$  ranging from 10 m to 35 m. For GPS / Galileo, curves of 99.9% availability coverage for  $\chi^2$  and SS RAIM are respectively displayed with a thick, solid line and with a dotted line with black diamond markers. In parallel, a thin, solid line and circular markers represent coverage for the system using all four constellations (GPS, Galileo, GLONASS, and Beidou). These preliminary results (not accounting for constellation faults, and assuming  $b_{MAX}=0$  m as mentioned in Table I) show that 100% availability is reached with either  $\chi^2$  or SS RAIM for  $\ell=25$ m using GPS/Galileo. For lower values of  $\ell$ ,  $\chi^2$  RAIM achieves significantly higher coverage than SS RAIM: for example, for  $\ell=20$ m, coverage reaches 99.6% using  $\chi^2$  RAIM versus 98.5% using SS RAIM. This improvement comes at the cost of substantially longer processing time for  $\chi^2$  RAIM, which was measured to be 4.5 times that of SS RAIM. The difference in coverage between  $\chi^2$  and SS RAIM FDE disappears when all four constellations are used, as shown by the overlapping thin, solid line and circular markers.

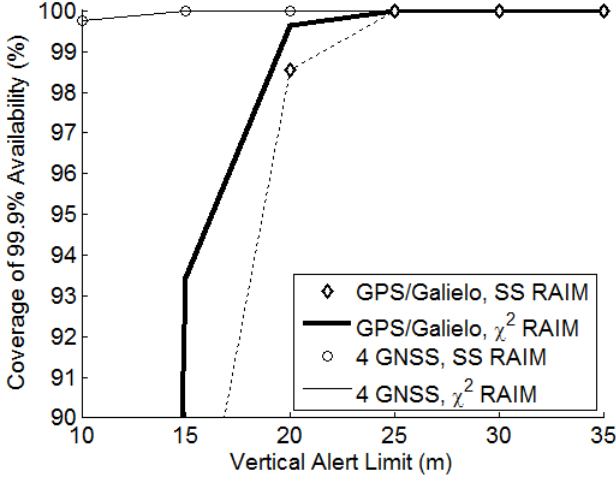


Fig. 11. Sensitivity of 99.9% availability coverage to alert limit, for  $b_{MAX}=0$ , using SS RAIM versus using  $\chi^2$  RAIM.

In future work, we will investigate the possibility of reducing the  $\chi^2$  RAIM computation load, for example using a more efficient line search algorithm to determine the worst-case fault magnitudes, or by deriving a new bound on the  $\chi^2$  RAIM FDE integrity risk.

## VI. CONCLUSION

The emergence of multi-constellation GNSS opens a new era in navigation integrity monitoring, which may no longer require costly ground infrastructure, but instead may be performed using RAIM.

In this paper, two new methods for fault detection and exclusion (FDE) were developed. A new chi-squared residual-based ( $\chi^2$ ) RAIM exclusion test statistic was defined based on parity space representations. It was shown that in parity space, the  $\chi^2$  RAIM no-detection and exclusion regions are hyperspherical and cylindrical, respectively, whereas for solution separation (SS) RAIM, they are polytopic and prismatic, respectively. Complete integrity and continuity risk equations were derived for both SS RAIM and  $\chi^2$  RAIM FDE, under hypotheses of single and multi-measurement faults.

A preliminary performance analysis was carried out for an example Advanced RAIM (ARAIM) application, assuming zero-mean nominal measurement errors, for vertical guidance of aircraft using GPS, Galileo, GLONASS and Beidou satellites. The paper showed that, on the one hand, the integrity risk bound was significantly tighter for the  $\chi^2$  approach as compared to SS RAIM, which resulted in much improved worldwide availability for  $\chi^2$  RAIM, especially when using two satellite constellations instead of four. On the other hand, the SS bound was designed to enable risk evaluation in practical implementations where computation resources are limited, which may not be possible using  $\chi^2$  RAIM FDE, whose processing time is almost five times larger than for SS RAIM.

## ACKNOWLEDGMENT

The authors would like to acknowledge Sooraj Kumar for his valuable contributions to the multi-constellation ARAIM availability simulation software.

## APPENDIX I. RESIDUAL-BASED EXPRESSION OF THE CHI-SQUARED RAIM EXCLUSION TEST STATISTIC

This appendix aims at proving that (50) and (52) are equivalent. In the first step of this three-step derivation, (50) is rewritten as:

$$\begin{aligned}
 q_{\perp,i} &= \mathbf{z}^T \mathbf{M}_{\perp,j}^T \mathbf{M}_{\perp,j} \mathbf{z} \\
 &= \mathbf{z}^T \mathbf{Q}^T [\mathbf{I}_{n-m} - \mathbf{U}_j \mathbf{U}_j^T]^T [\mathbf{I}_{n-m} - \mathbf{U}_j \mathbf{U}_j^T] \mathbf{Q} \mathbf{z} \\
 &= \mathbf{z}^T \mathbf{Q}^T \mathbf{Q} \mathbf{z} - \mathbf{z}^T \mathbf{Q}^T \mathbf{U}_j \mathbf{U}_j^T \mathbf{Q} \mathbf{z}
 \end{aligned} \quad (I.1)$$

where we used the fact that matrix  $\mathbf{U}_i \mathbf{U}_i^T$ , expressed as:

$$\mathbf{U}_i \mathbf{U}_i^T = \mathbf{Q} \mathbf{A}_i (\mathbf{A}_i^T \mathbf{Q}^T \mathbf{Q} \mathbf{A}_i)^{-1} \mathbf{A}_i^T \mathbf{Q}^T \quad (I.2)$$

is symmetric and idempotent.

Then, in a second step, (52) is written as:

$$\begin{aligned}
 q_{\perp,j} &= \mathbf{z}^T (\mathbf{I}_n - \mathbf{H} \mathbf{S}_0)^T [\mathbf{I}_n - \mathbf{R}_j]^T [\mathbf{I}_n - \mathbf{R}_j] (\mathbf{I}_n - \mathbf{H} \mathbf{S}_0) \mathbf{z} \\
 &= \mathbf{z}^T (\mathbf{I}_n - \mathbf{H} \mathbf{S}_0) \mathbf{z} - \mathbf{z}^T (\mathbf{I}_n - \mathbf{H} \mathbf{S}_0)^T \mathbf{R}_j (\mathbf{I}_n - \mathbf{H} \mathbf{S}_0) \mathbf{z} \\
 &= \mathbf{z}^T (\mathbf{I}_n - \mathbf{H} \mathbf{S}_0) \mathbf{z} - \mathbf{z}^T \mathbf{R}_j \mathbf{z}
 \end{aligned} \quad (I.3)$$

where we used the fact that  $\mathbf{R}_j$ , which is defined in (57), is symmetric and idempotent.

Finally, in the third step of derivation, the first and second terms in (I.1) and (I.2) are shown to be equivalent. The first terms are obviously equivalent because [10]:

$$\mathbf{Q}^T \mathbf{Q} = \mathbf{I}_n - \mathbf{H} \mathbf{S}_0 \quad (I.4)$$

The matrix in the second quadratic form on the right hand side in (I.2) can be expressed as:

$$\mathbf{Q}^T \mathbf{U}_j \mathbf{U}_j^T \mathbf{Q} = \mathbf{Q}^T \mathbf{Q} \mathbf{A}_j (\mathbf{A}_j^T \mathbf{Q}^T \mathbf{Q} \mathbf{A}_j)^{-1} \mathbf{A}_j^T \mathbf{Q}^T \mathbf{Q} \quad (I.5)$$

Substituting (I.4) into (I.5) and using the definition of  $\mathbf{R}_j$  in (57) shows that the second terms on the right hand side in (I.1) and (I.3) are equivalent, which concludes this proof.

## APPENDIX II. WORST-CASE FAULT VECTOR DIRECTION FOR THE CHI-SQUARED EXCLUSION TEST STATISTICS

This appendix provides a derivation of the worst-case fault vector direction  $\bar{\mathbf{f}}_{\perp,j,i}$ , which maximizes the exclusion term in the  $\chi^2$  integrity risk equation (54) under fault hypothesis  $H_i$ , after exclusion of subset measurement  $j$ . This derivation is similar to the one in [1], which defined the vector  $\bar{\mathbf{f}}_i$  that appears in (5) and (54).  $\bar{\mathbf{f}}_{\perp,j,i}$  designates the worst-case fault direction. The worst-case fault magnitude still needs to be treated separately using a straightforward search routine as described in the text.

Under  $H_i$ , the  $n_i \times 1$  vector  $\mathbf{f}_{A_i}$  of non-zero elements of the  $n \times 1$  fault vector  $\mathbf{f}$  is defined as:

$$\mathbf{f}_{A_i} \equiv \mathbf{A}_i^T \mathbf{f} \quad \text{such that} \quad \mathbf{f} = \mathbf{A}_i \mathbf{f}_{A_i} \quad (\text{II.1})$$

where  $\mathbf{A}_i$  is defined in (17).

Let  $g_{\perp,j,i}^2$  be the failure mode slope, i.e., the ratio of the mean squared of  $\varepsilon_j$  over the non-centrality parameter of  $q_{\perp,j}^2$ . Under  $H_i$ ,  $g_{\perp,j,i}^2$  can be written as:

$$g_{\perp,j,i}^2 = \frac{\mathbf{f}^T \mathbf{s}_j \mathbf{s}_j^T \mathbf{f}}{\mathbf{f}^T \mathbf{M}_{\perp,j}^T \mathbf{M}_{\perp,j} \mathbf{f}} \quad (\text{II.2})$$

Substituting (II.1) into (II.2), and using the following change of variables:

$$\mathbf{f}_{A_i} = \mathbf{M}_{A_i,j} \mathbf{f}_{A_i^*} \quad (\text{II.3})$$

(II.2) becomes

$$g_{\perp,j,i}^2 = \frac{\mathbf{f}_{A_i^*}^T \mathbf{M}_{A_i,j}^T \mathbf{m}_{X_{i,j}} \mathbf{m}_{X_{i,j}}^T \mathbf{M}_{A_i,j} \mathbf{f}_{A_i^*}}{\mathbf{f}_{A_i^*}^T \mathbf{M}_{A_i^*} \mathbf{f}_{A_i^*}} \quad (\text{II.4})$$

where,

$$\mathbf{m}_{X_{i,j}} = \mathbf{A}_i^T \mathbf{s}_j$$

$$\mathbf{M}_{A_i,j} = \left( \mathbf{A}_i^T \mathbf{M}_{\perp,j}^T \mathbf{M}_{\perp,j} \mathbf{A}_i \right)^{-1/2}$$

Using the residual-based expression in (52) and the definition of  $\mathbf{R}_j$  in (57),  $\mathbf{M}_{A_i,j}$  can also be written as:

$$\mathbf{M}_{A_i,j} = \left( \mathbf{A}_i^T \mathbf{R}_j \mathbf{A}_i \right)^{-1/2} \quad (\text{II.5})$$

It follows from (II.4) that the worst-case fault slope squared  $g_{\perp,j,i}^2$  under  $H_i$  is the maximum eigenvalue of the  $n_i \times n_i$

matrix [21]:

$$\mathbf{M}_{A_i,j}^T \mathbf{m}_{X_{i,j}} \mathbf{m}_{X_{i,j}}^T \mathbf{M}_{A_i,j} \quad (\text{II.6})$$

Let matrix  $\mathbf{M}$  be defined as:

$$\mathbf{M} \equiv \mathbf{M}_{A_i,j}^T \mathbf{m}_{X_{i,j}} \left( \mathbf{m}_{X_{i,j}}^T \mathbf{M}_{A_i,j} \mathbf{M}_{A_i,j}^T \mathbf{m}_{X_{i,j}} \right)^{-1} \mathbf{m}_{X_{i,j}}^T \mathbf{M}_{A_i,j} \quad (\text{II.7})$$

$\mathbf{M}$  is the  $n_i \times n_i$  matrix in (II.6) multiplied by the scalar ‘normalizing factor’  $(\mathbf{m}_{X_{i,j}}^T \mathbf{M}_{A_i,j} \mathbf{M}_{A_i,j}^T \mathbf{m}_{X_{i,j}})^{-1}$ . It can easily be shown that  $\mathbf{M}$  is symmetric and idempotent:

$$\mathbf{M} = \mathbf{M}^T \quad \text{and} \quad \mathbf{M} = \mathbf{M}\mathbf{M} \quad (\text{II.8})$$

Matrix  $\mathbf{M}$  is called an orthogonal projector and is derived from an outer product (because  $\mathbf{M}_{A_i,j}^T \mathbf{m}_{X_{i,j}}$  in (II.7) is a  $n_i \times 1$  vector). Therefore,  $\mathbf{M}$  has a single non-zero eigenvalue, of value 1. It follows that the matrix in (II.6) has a single non-zero eigenvalue, with value equal to the inverse of the normalizing factor used in (II.7). This provides an expression of the worst-case failure mode slope  $\bar{g}_{\perp,j,i}^2$ :

$$\bar{g}_{\perp,j,i}^2 = \mathbf{m}_{X_{i,j}}^T \mathbf{M}_{A_i,j} \mathbf{M}_{A_i,j}^T \mathbf{m}_{X_{i,j}} \quad (\text{II.9})$$

In addition, substituting  $\bar{g}_{\perp,j,i}^2$  for  $g_{\perp,j,i}^2$  in (II.4) and solving by inspection for  $\mathbf{f}_{A_i^*}$  shows that the direction of  $\mathbf{f}_{A_i^*}$  that maximizes  $g_{\perp,j,i}^2$  is aligned with vector  $\mathbf{M}_{A_i,j}^T \mathbf{m}_{X_{i,j}}$ . Thus, the conclusion of this appendix is that the worst-case fault direction  $\bar{\mathbf{f}}_{\perp,j,i}$  under a multi-measurement fault hypothesis  $H_i$  can be expressed analytically in a compact form as:

$$\bar{\mathbf{f}}_{\perp,j,i} = \mathbf{A}_i \mathbf{M}_{A_i,j} \mathbf{M}_{A_i,j}^T \mathbf{m}_{X_{i,j}} \quad (\text{II.10})$$

$$\text{i.e.,} \quad \bar{\mathbf{f}}_{\perp,j,i} = \mathbf{A}_i \left( \mathbf{A}_i^T \mathbf{M}_{\perp,j}^T \mathbf{M}_{\perp,j} \mathbf{A}_i \right)^{-1} \mathbf{A}_i^T \mathbf{s}_j$$

$$\text{or,} \quad \bar{\mathbf{f}}_{\perp,j,i} = \mathbf{A}_i \left( \mathbf{A}_i^T \mathbf{R}_j \mathbf{A}_i \right)^{-1} \mathbf{A}_i^T \mathbf{s}_j$$

where  $\mathbf{R}_j$  is defined in (57).

## APPENDIX III. PROOF OF INDEPENDENCE BETWEEN SUBSET ESTIMATE ERROR AND CHI-SQUARED RAIM EXCLUSION TEST STATISTIC

This appendix proves the independence between the subset estimate error  $\varepsilon_j$  and the  $\chi^2$  RAIM exclusion test statistic  $q_{\perp,j}$ . The derivation starts by showing that  $\varepsilon_j$  and  $\mathbf{q}_{\perp,j}$  are uncorrelated. The correlation matrix between  $\varepsilon_j$  and  $\mathbf{q}_{\perp,j}$  is expressed as:

$$E\{\mathbf{q}_{\perp,j}\boldsymbol{\varepsilon}_j^T\} = (\mathbf{I}_{n-m} - \mathbf{U}_j\mathbf{U}_j^T) \mathbf{Q} \mathbf{S}_j^T \boldsymbol{\alpha} \quad (\text{III.1})$$

where

$$\mathbf{S}_j = \mathbf{P}_j \mathbf{H}^T \mathbf{B}_j \mathbf{B}_j^T$$

Substituting (48) into (III.1), the following equation is obtained:

$$E\{\mathbf{q}_{\perp,j}\boldsymbol{\varepsilon}_j^T\} = (\mathbf{I}_{n-m} - \mathbf{Q}\mathbf{A}_j(\mathbf{A}_j^T\mathbf{Q}^T\mathbf{Q}\mathbf{A}_j)^{-1}\mathbf{A}_j^T\mathbf{Q}^T) \mathbf{Q} \mathbf{B}_j \mathbf{B}_j^T \mathbf{H} \mathbf{P}_j \boldsymbol{\alpha}$$

Pre-multiply both sides of the above equation by  $\mathbf{A}_j^T\mathbf{Q}^T$  and expanding shows that:

$$\mathbf{A}_j^T\mathbf{Q}^T E\{\mathbf{q}_{\perp,j}\boldsymbol{\varepsilon}_j^T\} = \mathbf{0}_{n_j \times 1} \quad (\text{III.2})$$

which proves that:

$$E\{\mathbf{q}_{\perp,j}\boldsymbol{\varepsilon}_j^T\} = \mathbf{0}_{(n-m) \times 1} \quad (\text{III.3})$$

Equation (III.3) shows that the least-squares estimate error  $\boldsymbol{\varepsilon}_j$  is uncorrelated with  $\mathbf{q}_{\perp,j}$ .  $\boldsymbol{\varepsilon}_j$  and  $\mathbf{q}_{\perp,j}$  are also jointly normally distributed. Therefore, all elements of  $\mathbf{q}_{\perp,j}$  are linearly independent from  $\boldsymbol{\varepsilon}_j$ , which ensures that any combination of these elements (including the norm  $q_{\perp,j}$  of  $\mathbf{q}_{\perp,j}$  for  $\chi^2$  RAIM) is statistically independent from  $\boldsymbol{\varepsilon}_j$ .

#### REFERENCES

- [1] M. Joerger, S. Stevanovic, F.C. Chan, S. Langel, and B. Pervan, "Integrity Risk and Continuity Risk for Fault Detection and Exclusion Using Solution Separation ARAIM," *Proc. of ION GNSS+ 2013*, Nashville, TN, September 2013, pp. 2702-2722.
- [2] Y.C. Lee, "Analysis of Range and Position Comparison Methods as a Means to Provide GPS Integrity in the User Receiver," *Proc. of the 42nd Annual Meeting of The ION*, Seattle, WA, 1986, pp. 1-4.
- [3] B.W. Parkinson, and P. Axelrad, "Autonomous GPS Integrity Monitoring Using the Pseudorange Residual," *NAVIGATION*, Washington, DC, vol. 35, no. 2, 1988, pp. 225-274.
- [4] J. Blanch, T. Walter, T. Lee, B. Pervan, M. Rippl, and A. Spletter, "Advanced RAIM User Algorithm Description: Integrity Support Message Processing, Fault Detection, Exclusion, and Protection Level Calculation," *Proc. of ION GNSS 2012*, Nashville, TN, Sept. 17-21, 2012, pp. 2828 - 2849.
- [5] J. Blanch et al., "Critical Elements for a Multi-Constellation Advanced RAIM," *NAVIGATION*, vol. 60, no. 1, Spring 2013, pp. 53-69.
- [6] F. van Graas, J. Farrell, "Baseline Fault Detection and Exclusion Algorithm," *Proc. of the 49th Annual Meeting of The ION*, Cambridge, MA, June 1993, pp. 413-420.
- [7] B. Pervan, D. Lawrence, C. Cohen, and B. Parkinson, "Parity Space Methods for Autonomous Fault Detection and Exclusion Using GPS Carrier Phase," *Proc. of IEEE PLANS*, Atlanta, GA, 1996.
- [8] M. Brenner, "Integrated GPS/Inertial Fault Detection Availability," *NAVIGATION*, vol. 43, no. 2, Summer 1996, pp. 111-130.
- [9] J. Wang, and P. Ober, "On the Availability of Fault Detection and Exclusion in GNSS Receiver Autonomous Integrity Monitoring," *The J. of Navigation of the RIN*, vol. 62, 2009.
- [10] Potter, I. E., and Sunman, M. C., "Threshold-less Redundancy Management With Arrays of Skewed Instruments," *AGARDOGRAPH - No 224*, 1977, pp 15-11 to 15-25.
- [11] M. Joerger, F.C. Chan, S., Langel, and B. Pervan, "RAIM Detector and Estimator Design to Minimize the Integrity Risk," *Proc. of ION GNSS 2012*, Nashville, TN, September 2012, pp. 2785-2807.
- [12] RTCA Special Committee 159, "Minimum Aviation System Performance Standards for the Local Area Augmentation System (LAAS)," *RTCA/DO-245*, 2004, Appendix D.
- [13] M. Sturza, "Navigation System Integrity Monitoring Using Redundant Measurements," *NAVIGATION*, Washington, DC, vol. 35 no. 4, 1988, pp. 69-87.
- [14] J. Blanch, A. Ene, T. Walter, and P. Enge, "An Optimized Multiple Hypothesis RAIM Algorithm for Vertical Guidance," *Proc. of ION GNSS 2007*, Fort Worth, TX, September 2007, pp. 2924-2933.
- [15] M. Joerger, F.C. Chan, and B. Pervan, "Solution Separation Versus Residual-Based RAIM," *NAVIGATION*, in press.
- [16] C.D. Meyer, *Matrix Analysis and Applied Linear Algebra*, Society for Industrial and Applied Mathematics, 2000.
- [17] J. Blanch, T. Walter, and P. Enge, "Results on the Optimal Detection Statistic for Integrity Monitoring," *Proc. of ION ITM 2013*, San Diego, CA, January 2013, pp. 262-273.
- [18] RTCA Special Committee 159, "Minimum Operational Performance Standards for Global Positioning System/Wide Area Augmentation System Airborne Equipment," *Document No. RTCA/DO-229C*, Washington, DC., 2001
- [19] J.P. Boyero: personal conversation within the ARAIM working group C
- [20] almanac files provided by Stanford University, available online at <http://waas.stanford.edu/staff/maast/maast.html>
- [21] Angus, J. E., "RAIM with Multiple Faults", *NAVIGATION*, Vol. 53, No. 4, Winter 2006-2007, pp. 249-257.